An Integrated Control Algorithm for a Single-Stage PV Pumping System Using an Open-End Winding Induction Motor

Sachin Jain, *Member, IEEE*, Ramsha Karampuri, and V. T. Somasekhar, *Member, IEEE*

***Abstract*—In this paper, a single-stage solution for solar photovoltaic (PV) pumping system using a dual-inverter fed open-end winding induction motor drive is presented. The three-level dual-inverter requires a low PV bus voltage compared with its conventional three-level counterpart. This could avoid large string of PV modules and helps in reducing the voltage rating of the capacitors and semiconductor devices used in the system. This may further help in reduction of cost of the system. The proposed single-stage system is operated using an integrated control algorithm, which includes the maximum power point tracking (MPPT), the V/f control, and the sample-averaged zero-sequence elimination (SAZE) pulsewidth modulation (PWM) technique. While the MPPT algorithm ensures the extraction of maximum power from the PV source, the V/f control improves the motor pump performance. Furthermore, the zero-sequence current is avoided by the SAZE PWM algorithm. Thus, the integrated control algorithm improves the overall performance of the system. Furthermore, this paper also presents the details of system design and analysis of its dynamic behavior during transient environmental conditions. The performance of the system is verified using MATLAB simulation and hardware prototype.**

***Index Terms*—Dual inverter, maximum power point tracking (MPPT), open-end winding induction motor (OEWIM), photovoltaic (PV) cell, single-stage system.**

I. Introduction

ENORMOUS research work is being reported on multilevel inverter drives ever since Nabae *et al.* [1] introduced the three-level inverter. The three-level neutral-point-clamped (NPC) inverter is advantageous over the two-level H-bridge inverter as it has the benefits of low electromagnetic interference and high power quality, which improves the overall performance of the drive systems [2]. There is another alternative to the three-level NPC inverter drive, which is suggested by Stemmler and Guggenbach [3], using two two-level inverters (dual inverter) connected to either ends of an open-end winding induction motor (OEWIM). Thereafter, vast work is being carried out on various converter topologies [4]–[7] and pulse width modulation (PWM) techniques [8]–[11] for OEWIM drive. Most recently, the multiphase induction motor drives for high-power applications are also being studied using OEWIM topology [12], [13].

The advantages offered by the three-level dual-inverter fed OEWIM drive over the conventional NPC three-level inverter are well documented in [14]. These advantages include the absence of neutral point fluctuations and the requirement of lower dc bus voltage. It is envisaged that this drive, which is coupled to a centrifugal pump, could be employed for pumping applications. Of the available pump drive systems, the water pump drive systems are most commonly used in industries, agriculture, and multistoried buildings. In these applications, water from the ground or canal can be stored and used later whenever necessary. Thus, variations in the flow rate of water from the pump could be considered to be acceptable. Hence, a solar-powered water pump drive seems to be an attractive proposition owing to its renewable nature, zero pollution, and maintenance-free operation.

Many investigations have been reported on two-stage and single-stage PV-powered pumping systems [15]–[20]. Several investigations used a two-level inverter to drive the conventional induction motor pump [16]–[18], as shown in Fig. 1(a). To improve the system performance further, a three-level NPC inverter is used in the recent work, which is presented in [19] and [20]. However, the three-level NPC inverter has the disadvantages as discussed in the previous paragraph, and it requires excessive number of clamping diodes compared with a three-level dual inverter.

This paper presents an alternative solution for a single-stage PV pumping system using a three-level dual-inverter fed OEWIM pump, as shown in Fig. 1(b). The key features and advantages of the proposed system are as follows.

1) It is a single-stage system wherein the maximum power point tracking (MPPT) and the motor control are simultaneously achieved by an integrated control algorithm.
2) The proposed control algorithm can maintain the system stability by forcing the operation toward the voltage source region of $P-V$ curve even under worst environmental conditions.

Manuscript received February 28, 2015; revised June 22, 2015; accepted July 15, 2015. Date of publication September 22, 2015; date of current version January 8, 2016.

The authors are with the Department of Electrical Engineering, National Institute of Technology, Warangal 506 004, India (e-mail: jsachin@nitw.ac.in; s_binayake@rediffmail.com).

Color versions of one or more of the figures in this paper are available online at http://ieeexplore.ieee.org.

Digital Object Identifier 10.1109/TIE.2015.2480765

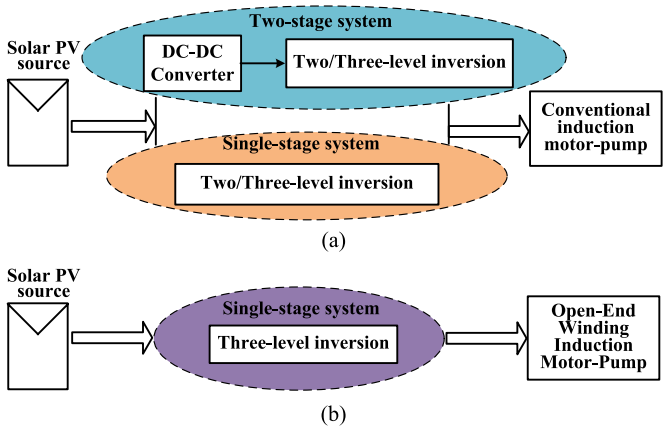

Fig. 1. Block diagram of PV-powered centrifugal pump system (a) with conventional induction motor and (b) with OEWIM.

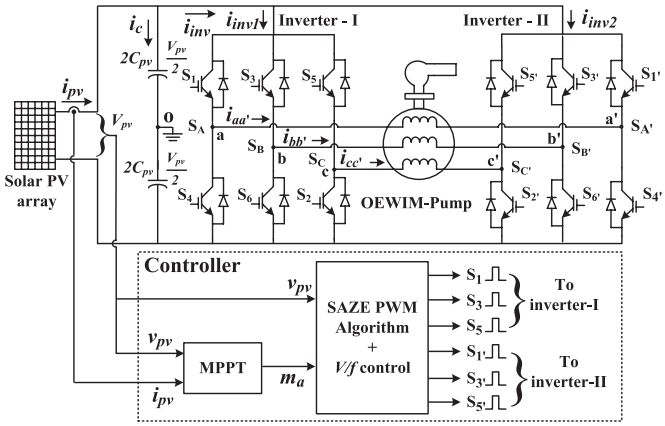

Fig. 2. Schematic circuit diagram of the proposed system.

3) The proposed system requires low value of PV/dc bus voltage, which reduces the voltage rating and size of PV bus capacitor and the power semiconductor devices.

The rest of this paper is divided into four sections. Section II describes the design and operational principles of the proposed system. Section III presents a detailed analysis along with the simulation results. Experimental validation of the proposed system is presented in Section IV.

II. Working Principle, Design, and Operation of the Proposed System

The circuit schematic of the proposed system is shown in Fig. 2. It consists of two two-level inverters whose outputs are connected to six terminals of an OEWIM coupled to a pump load. The inverters are switched using the sample-averaged zero-sequence elimination (SAZE) PWM algorithm, which controls the input phase voltage of the OEWIM. This algorithm alternatively clamps the output of one inverter and switches the other with high frequency to obtain the required phase voltage. Clamping an inverter reduces the switching losses in the system. The SAZE PWM algorithm is integrated with the MPPT algorithm and the V/f control to achieve maximum output from the system and the PV source. Furthermore, as life of PV source is high (≈20 years), special care is required in the design of the system. Therefore, components and devices should be chosen critically, particularly the PV bus capacitor. The detailed design of the system is given in the next subsection.

TABLE I
Motor and Solar PV Module Parameters

Parameter	Value	Parameter	Value
Motor parameters			
Rated phase voltage (RMS)	230 V	Frequency	50 Hz
Rated speed	1430 rpm	Poles, P	4
Stator winding resistance, r_s	1.405 Ω	Rotor winding resistance, r_r	1.395 Ω
Leakage reactance, $x_{ls} = x_{lr}$	1.8344 Ω	Magnetizing reactance, x_m	54.1 Ω
PV module parameters [21]			
Insolation	1 Sun	Temperature	25°C
Maximum power, P_{max}	59.9 W	Number of modules in the array	20 x 3
Open-circuit voltage, V_{oc}	21 V	Short-circuit current, I_{sc}	3.74 A
Voltage at maximum power	17.1 V	Current at maximum power	3.5 A

A. PV System Design

For simulating the proposed system using MATLAB/Simulink, a three-phase 4-kW OEWIM is taken keeping the requirement of centrifugal pump load in mind. The power delivered to the OEWIM is determined by the PV array power. In addition, the phase voltage $V_{aa'}$ of the OEWIM decides the maximum required operating voltage for the PV modules [21] to be connected in series (details of which are given in Table I). The modulation index of the dual-inverter system is defined as

$$m_a = \frac{|V_{sr}|}{V_{\rm dc}} \tag{1}$$

where $|V_{sr}|$ is the magnitude of the reference voltage space vector, and $V_{\rm dc}$ is the input dc bus voltage. For the proposed system, $V_{\rm dc} = 2V_{\rm pv}$ as the output of the PV array is given as the input of the dual inverter. The PV bus voltage required to generate the rated phase voltage using the three-level dual inverter is

$$\frac{2}{3} m_{a,\max} V_{\rm pv} = \frac{\sqrt{2} V_{aa'}}{2} \Rightarrow V_{\rm pv} = \sqrt{2} \times 230 = 325 \text{ V} \tag{2}$$

where $m_{a,\max}$ is the maximum modulation index, which assumes a value of 0.75 for the dual-inverter system with the SAZE PWM technique [14]. Assuming the derived operating voltage to be optimum for meeting the power requirement, the open-circuit voltage $V_{\rm oc}$ of the PV panel is designed for 1.3 times the PV bus voltage [22]. Thus,

$$V_{\rm oc} = 1.3\, V_{\rm pv} = 422.5 \text{ V}. \tag{3}$$

The low value of the PV bus voltage $V_{\rm pv}$ given in (2) helps in the optimum arrangement of PV modules for better performance and efficiency.

B. Dual-Inverter Design

The dual-inverter system shown in Fig. 2 consists of 12 power semiconductor switches. Each switch should block the complete PV bus voltage $V_{\rm pv}$ (firmly $V_{\rm oc}$) when its counterpart is in conducting state. Hence, the nominal voltage rating of the semiconductor switches is

$$V_{\rm sw} = V_{\rm oc} = 422.5 \text{ V}. \tag{4}$$

Similarly, each switch of the inverter should carry the load current supplied by the PV source when the switch is in ON-state. Thus, the inverter current $i_{\rm inv}$ (see Fig. 2) supplied by the PV source can be expressed as

$$i_{\rm inv} = (S_A - S_{A'})i_{aa'} + (S_B - S_{B'})i_{bb'} + (S_C - S_{C'})i_{cc'} \tag{5}$$

where $i_{aa'}, i_{bb'}$, and $i_{cc'}$ are the instantaneous current flowing through the motor phases $aa', bb',$ and cc', respectively; and $S_x (x \in \{A, B, C, A', B', C'\})$ is the switching function defined for all the six poles a, b, c, a', b', and c' of the dual inverter. The switching function S_x holds the value "1" when the upper switch of the pole is ON and "0" when it is OFF.

The current rating of the switch for a given pole (for example, pole "a") is determined by the peak current carried by that load phase. The peak value of current flowing through the switch, i.e., $\hat{i}_{\rm sw}$, is given by

$$\hat{i}_{\rm sw} = (S_A - S_{A'})\hat{i}_{aa'} \tag{6}$$

where $\hat{i}_{aa'}$ is the rated peak value of motor phase current ($\approx$10.2 A for the 4-kW OEWIM).

Using (4) and (6), the power semiconductor device with 450-V 15-A rating can be chosen for the dual inverter in the proposed system.

C. PV Bus Capacitor Design

As the PV bus voltage required in the proposed system is reduced nearly by half [see (2)], the voltage rating of the PV bus capacitor also reduces. The capacitance value is designed based on the ripple current that has to be carried by the capacitor, i.e., i_c, which is given by

$$i_c = i_{\rm pv} - i_{\rm inv} \tag{7}$$

where $i_{\rm pv}$ is the current supplied by the PV source (i.e., $3.74 \times 3 = 11.22$ A, from Table I).

To calculate the ripple in the capacitor current, the worst case is considered at which $i_{\rm inv}$ is zero. With the SAZE PWM scheme, such a worst case occurs when inverter I and inverter II of the dual inverter assume same switching state (for example, $\{S_A, S_B, S_C\} = \{S_{A'}, S_{B'}, S_{C'}\} = \{0, 1, 0\}$). Hence, from (7),

$$i_{c,\max} = 11.22 \text{ A}. \tag{8}$$

The capacitance needed would be then given by

$$C_{\rm pv} = \frac{i_{c,\max}}{f_s \Delta V_{\rm pv}} \tag{9}$$

where f_s is the frequency at which the semiconductor switches are operated, and $\Delta V_{\rm pv}$ is the ripple content in the PV bus voltage. Considering $\Delta V_{\rm pv}$ to be 2% of the PV bus voltage (i.e., $V_{\rm oc} \times 0.02 = 8.4$ V), the lowest switching frequency should be 1.28 kHz for maximum possible capacitance value (corresponding to the minimum modulation index $m_a = 0.2$ and 96 samples per fundamental cycle of inverter output voltage), and substituting $i_{c,\max}$ from (8) into (9) results in

$$C_{\rm pv} = 1043 \ \mu\text{F} \approx 1100 \ \mu\text{F}. \tag{10}$$

Thus, a capacitor of 450 V, 15 A, 1100 μF can serve the need of the proposed system.

D. Integrated Control Algorithm

The aforementioned designed single-stage PV pumping system is operated with an integrated control algorithm, which consists of MPPT and SAZE PWM techniques along with V/f control. The flow of the control algorithm is presented in Fig. 3 and is explained in the following.

MPPT algorithm: The hill climbing algorithm, one of the simplest, popular, and commercially used methods of MPPT [22], [23], is employed in the proposed system. As shown in the first part in Fig. 3, i.e., the MPPT section, the instantaneous values of PV array voltage $v_{\rm pv}$ and PV array current $i_{\rm pv}$ are fed into the MPPT algorithm. Before feeding $v_{\rm pv}$ and $i_{\rm pv}$ to the MPPT controller, they are passed through a low-pass filter to filter the noise. The PV array power $P_{\rm pv}$ is then calculated using the sensed averaged values of $V_{\rm pv}$ and $I_{\rm pv}$ output by the low-pass filter. Then, by comparing the present PV power and voltage with their previous available values, the slope of operating point on PV curve is determined. The sign (positive or negative value) of the slope determines the modification for modulation index m_a. Based on the sign of the slope (negative or positive), the value of m_a is modified (increased or decreased, respectively) as follows:

$$m_a = m_a \pm \Delta m_a \tag{11}$$

where Δm_a is the step change in m_a.

The calculated value of m_a is then used by the V/f control and the SAZE PWM algorithm to operate the dual inverter connected to the OEWIM pump, which can extract maximum power available from the PV source.

SAZE PWM Algorithm: The basic PWM algorithm used in this work is based on the concept of imaginary switching time periods and the effective time $T_{\rm eff}$ [24], [25]. This space vector PWM algorithm is adopted for the dual-inverter fed OEWIM drive [14], wherein the zero-sequence current is suppressed by the relocation of the effective time period within a sampling time interval. This technique, which is named as SAZE PWM, is presented in the form of an algorithm in the second part in Fig. 3 and is briefly explained in the following.

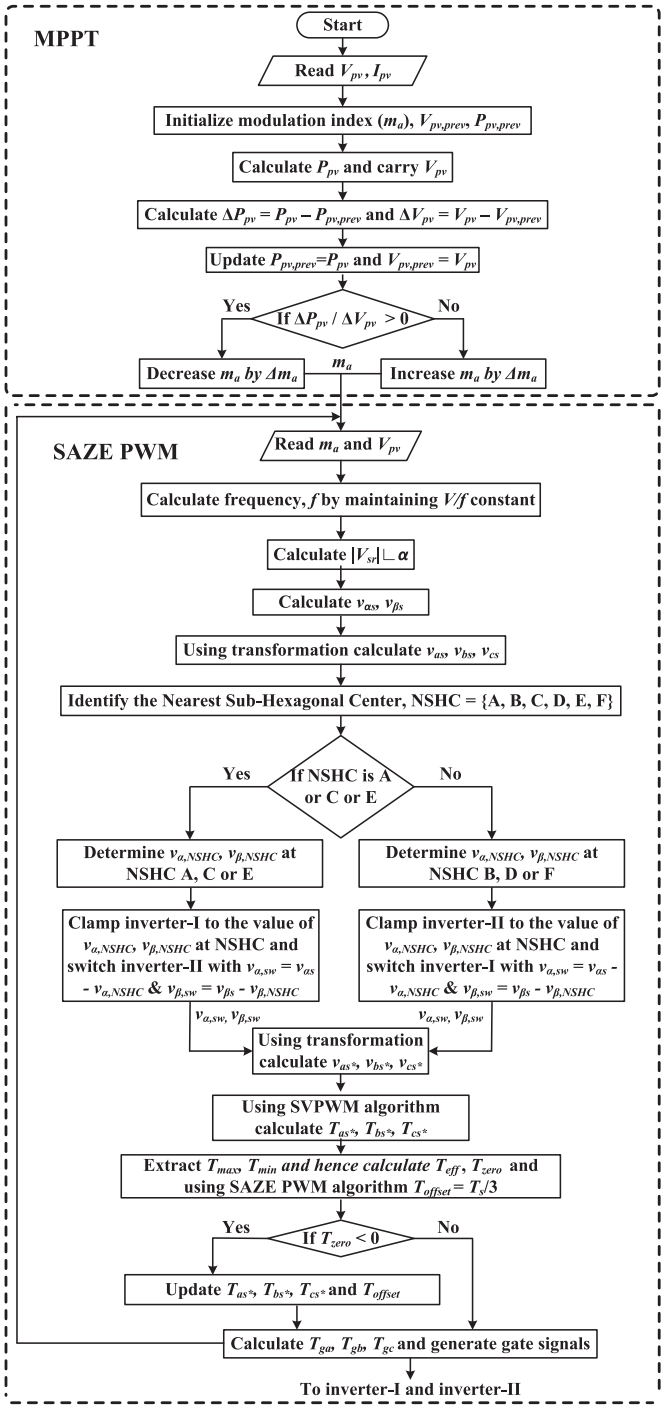

Fig. 3. Flowchart of the integrated control algorithm.

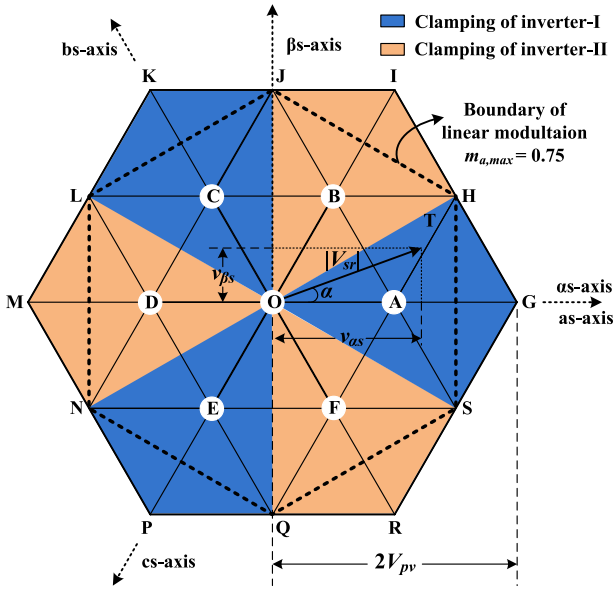

Fig. 4. Space vector locations for the dual inverter with the combination of inverter I and inverter II switching states.

TABLE II
VOLTAGE VECTOR MAGNITUDES AT ALL THE NSHCS

NSHC	Clamping inverter-I			Clamping inverter-II		
Vector	A	C	E	B	D	F
$v_{\alpha,NSHC}$	V_{pv}	-0.5 V_{pv}	-0.5 V_{pv}	$0.5V_{pv}$	$-V_{pv}$	0.5 V_{pv}
$v_{\beta,NSHC}$	0	0.867 V_{pv}	-0.867 V_{pv}	0.867 V_{pv}	0	-0.867 V_{pv}

Inverter I and inverter II of the dual inverter shown in Fig. 2 are the two-level inverters, which are combined to generate three-level motor phase voltages $v_{aa'}, v_{bb'}, v_{cc'}$. Each inverter individually can produce the phase voltage with a peak value of $V_{\rm pv}$ (OA) and together can produce $2V_{\rm pv}$ (OG), as shown in Fig. 4. In Fig. 4, A, B, C, D, . . ., S represents the space vector locations, and each equilateral subtriangle is a sector. The space vector locations A, C, and E are considered as nearest subhexagonal centers (NSHCs) for inverter I to be clamped to the magnitude of $v_{\alpha,\rm NSHC}$ and $v_{\beta,\rm NSHC}$, while inverter II is switched with high frequency. Similarly, the locations B, D, and F are considered as NSHCs for inverter II to be clamped to the magnitude of $v_{\alpha,\rm NSHC}$ and $v_{\beta,\rm NSHC}$, while inverter I is switched. Two different shades shown in Fig. 4 represent the region for clamping either inverter I or inverter II. The values of $v_{\alpha,\rm NSHC}$ and $v_{\beta,\rm NSHC}$ for all the NSHCs for inverter I and inverter II, when they are clamped, are furnished in Table II.

In Fig. 4, the magnitude of the reference voltage vector OT ($|v_{sr}|$) is dependent on the value of m_a as given in (1), which is generated by MPPT block depending on the insolation (G) and temperature (T).

The angle "α" (see Figs. 3 and 4) is the function of the fundamental frequency f of the motor phase voltage, where the value of f is calculated using m_a as follows:

$$f = \frac{m_a f_{\rm rated}}{m_{a,\max}} \tag{12}$$

where $f_{\rm rated}(= 50$ Hz) is the fundamental frequency of the motor phase voltage at and above the boundary of linear modulation.

The value of m_a decides the magnitude of reference voltage and its fundamental frequency and hence the ratio V/f, so that the motor always maintains the rated air-gap flux. This could improve the performance of the OEWIM pump drive by generating the highest possible torque at various environmental conditions. Furthermore, the performance of the proposed system is analyzed for various environmental conditions using the simulation studies presented in the next section.

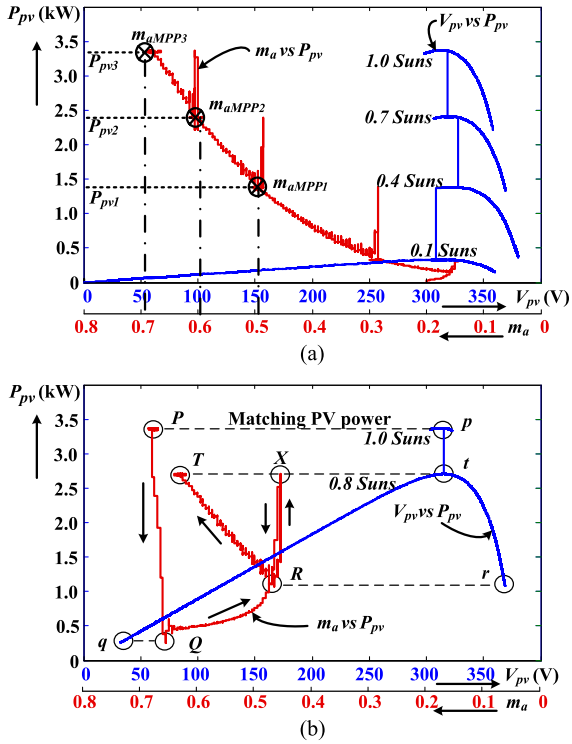

Fig. 5. $V_{\rm pv}$ versus $P_{\rm pv}$ and m_a versus $P_{\rm pv}$ characteristics (a) for increasing insolation and (b) for decreasing insolation (along with slight variation in temperature).

III. Analysis and Simulation of the Proposed System

The simulation of the proposed single-stage PV pumping system is performed using MATLAB/Simulink with the following assumptions.

1) The OEWIM pump is operated with V/f control at and above 10% of its rated speed.
2) The flux generated in the air gap of the OEWIM is always at its rated value.
3) As the envisaged application is pumping, the mechanical torque generated by the OEWIM is proportional to the square of the motor speed.
4) The dual-inverter system is lossless.

A. Dynamic Analysis of the Proposed PV System With Integrated Algorithm

In addition to the aforementioned assumptions, the following points are to be noted for the simplification of analysis of the proposed system.

1) The value of m_a corresponding to maximum power point (MPP) at a particular insolation and temperature is constant and is denoted by $m_{a\rm MPP}$.
2) The PV voltage $V_{\rm pv}$ at MPP is assumed to be nearly constant for various environmental conditions (with slight variation in operating temperature).
3) The value of $m_{a\rm MPP}$ is assumed to be in linear relationship with the PV power, which can be observed from Fig. 5(a), where the ratio of $m_{a\rm MPP1}$, $m_{a\rm MPP2}$, and $m_{a\rm MPP3}$ to $P_{\rm pv1}$, $P_{\rm pv2}$ and $P_{\rm pv3}$, respectively, is nearly equal. Thus,

$$m_{a\rm MPP} \propto P_{\rm pv} \tag{13}$$

$$\Rightarrow m_{a\rm MPP} \approx K_1 P_{\rm pv} \tag{14}$$

where K_1 is a constant.

Furthermore, considering the motor pump side, the frequency of phase quantities applied to the motor is proportional to m_a, as given in (12), and can be written as

$$\omega_s \propto m_{a\rm MPP} (\because \omega_s = 2\pi f) \tag{15}$$

$$\Rightarrow \frac{\omega_r}{(1-s)} \propto m_{a\rm MPP} \tag{16}$$

where ω_s is the synchronous speed (rad/s) of the motor, ω_r is the rotor speed, and s is the slip.

The centrifugal pump connected to the OEWIM holds the *affinity laws* as follows:

$$Q \propto \omega_r;\ H \propto \omega_r^2;\ P_{\rm Elect} \propto \omega_r^3 \tag{17}$$

where Q is the flow rate ($\rm m^3/s$), and H is the head (m).

Relating the OEWIM input power $P_{\rm Elect}$ with $m_{a\rm MPP}$ using (16) and (17) results in the proportionality

$$P_{\rm Elect} \propto (m_{a\rm MPP})^3 (1-s)^3 \tag{18}$$

$$P_{\rm Elect} \approx K_2 (m_{a\rm MPP})^3 (1-s)^3 \tag{19}$$

where K_2 is a constant.

As the dual inverter is assumed to be ideal, $P_{\rm pv}$ and $P_{\rm Elect}$ can be equated to deduce the relation between $m_{a\rm MPP}$ and slip s as follows:

$$P_{\rm pv} = P_{\rm Elect} \tag{20}$$

$$\Rightarrow \left(\frac{1}{K_1}\right) m_{a\rm MPP} = K_2 (m_{a\rm MPP})^3 (1-s)^3 \tag{21}$$

$$\Rightarrow K_3 = (m_{a\rm MPP})^2 (1-s)^3 \tag{22}$$

where $K_3 = 1/(K_1 K_2)$ and is a constant.

From (22), it can be concluded that, for a change in the value of $m_{a\rm MPP}$, there will be a corresponding change in the motor slip s and hence the slip power. The change (increase) in the slip power can be also observed from Fig. 6(a) (i.e., the power difference between $P_{\rm pv}$ and $P_{\rm Elect}$ is the slip power, since inverter losses are neglected). In addition, from (19) it can be concluded that, for increase (decrease) in $m_{a\rm MPP}$ and s, the value of $P_{\rm Elect}$ also increases (decreases), as shown in Fig. 6(a). In addition, the increment in $P_{\rm Elect}$ is gentle when compared with $P_{\rm pv}$, because $m_{a\rm MPP}$ and s are decimal numbers (varying between 0 and 1). In addition, the increment of $P_{\rm Elect}$ is steeper at the MPP because of the mechanical time constant of the motor pump set.

Furthermore, few more important observations can be made from Figs. 5(b) and 6(b), where the plots for reduced insolation are presented. In Fig. 5(b), the operating point $P(p)$ corresponds to insolation 1 Sun, and it shifts to $T(t)$ when the insolation is reduced to 0.8 Suns. At the instant when insolation

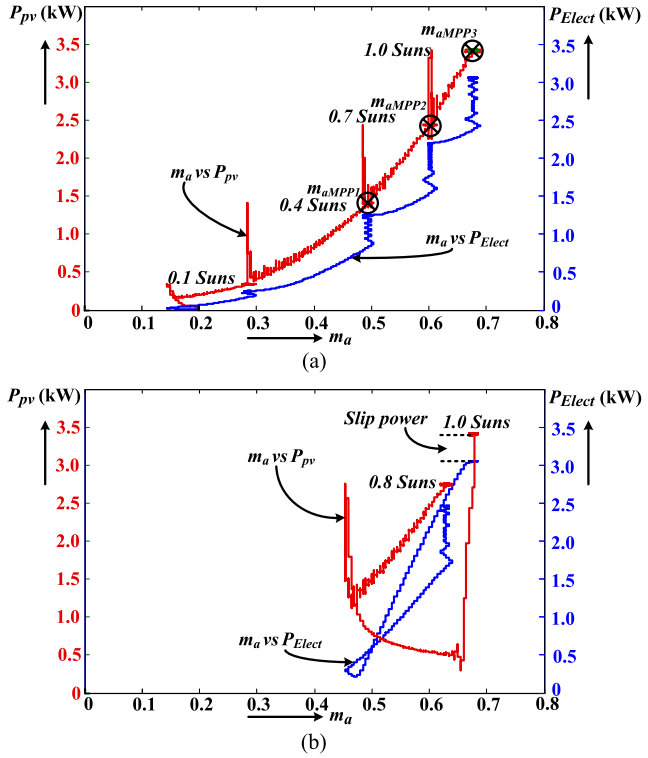

Fig. 6. m_a versus $P_{\rm pv}$ and m_a versus $P_{\rm Elect}$ characteristics (a) for increasing insolation and (b) for decreasing insolation (along with slight variation in temperature).

is reduced suddenly, the motor power demand is more than the generated PV power. Thus, the PV bus capacitor discharges to serve the need, and hence, the PV bus voltage falls down to $Q(q)$. The algorithm reduces the value of m_a (from Q to R) to rebuild the PV bus voltage (from q to t) and then tracks the maximum power (from R to T). The point X in the m_a versus $P_{\rm pv}$ curve is because, when the algorithm forces m_a to shift the operation toward the voltage source region, it traverses through the MPP.

Thus, the modulation index relates both the PV power and the motor power as discussed earlier, and it takes care of the nonlinearity between them. To conclude, the modulation index always maintains the stability of the system under all the environmental conditions, either increasing or decreasing.

B. Simulation Results of the PV Pumping System at PV Source Side and Load Side

With the aforementioned assumptions, the proposed single-stage PV pumping system using OEWIM is simulated for various possible (also worst) insolation and temperature conditions. The Simulink model of the proposed system is built in MATLAB using the following equations.

The PV module is realized by using the PV *current–voltage* characteristic equation presented in [21] and is given by

$$I_{\rm pv} = I_L - I_0 \left(e^{\frac{q(V_{\rm pv}+I_{\rm pv}R_s)}{nkT}} - 1 \right) \tag{23}$$

where $I_{\rm pv}$ is the current of the PV module, I_L is the photocurrent, I_0 is the diode saturation current, n is the diode quality

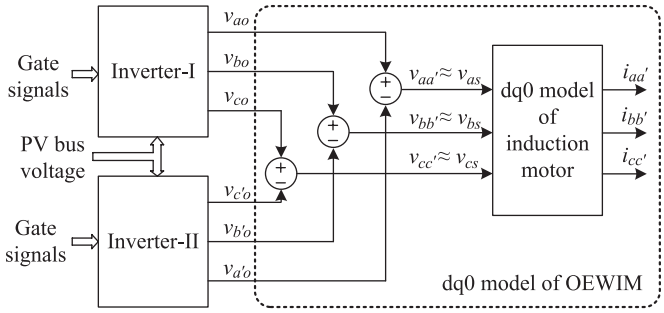

Fig. 7. $dq0$ model of OEWIM along with the dual inverter [26].

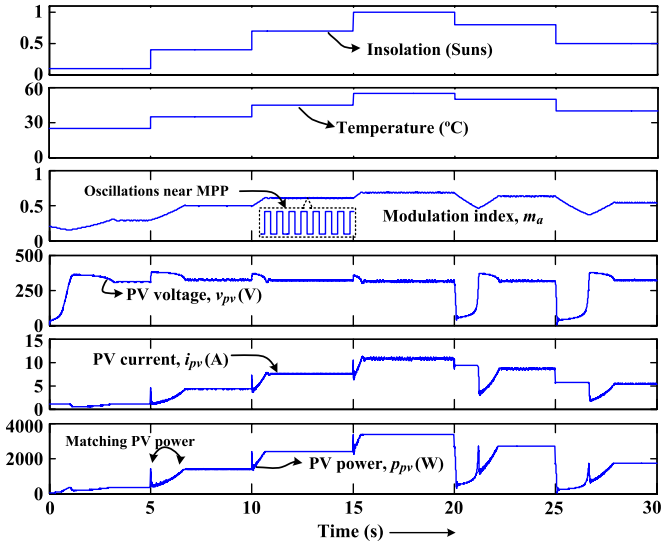

Fig. 8. PV-source-side waveforms from simulation.

or ideality factor, k is the Boltzmann constant, q is the electron charge, T is the module operating temperature in kelvins, R_s is the series resistance, and $V_{\rm pv}$ is the PV module voltage.

The OEWIM model [26] is developed by using the popular $dq0$ model of an induction motor and is shown in Fig. 7. The two two-level inverters (inverter I and inverter II) shown in Fig. 7 use ideal switches. In addition, the model for centrifugal pump uses the affinity laws as given by (17).

The simulation results for the PV-source-side, motor-side, and centrifugal-pump-side parameters are shown in Figs. 8–10, respectively. The simulation is performed by considering two worst cases: one is the condition of very low insolation i.e., 0.1 Suns, and the other is the step increase/decrease in the insolation and temperature. The simulation results demonstrate the satisfactory performance of the proposed system even in these worst situations.

In Fig. 8, the changing nature of PV power with respect to insolation and temperature by changing the value of m_a verifies the MPPT. Small oscillations in the value of m_a near MPP and the ripple content in the PV power confirm the operation near optimum voltage. In addition, for every step increase or decrease in insolation and temperature, the operating voltage of PV array passes through the optimum voltage. This can be justified with the matching values of peak power during transient tracking and steady state near MPP as given in the PV

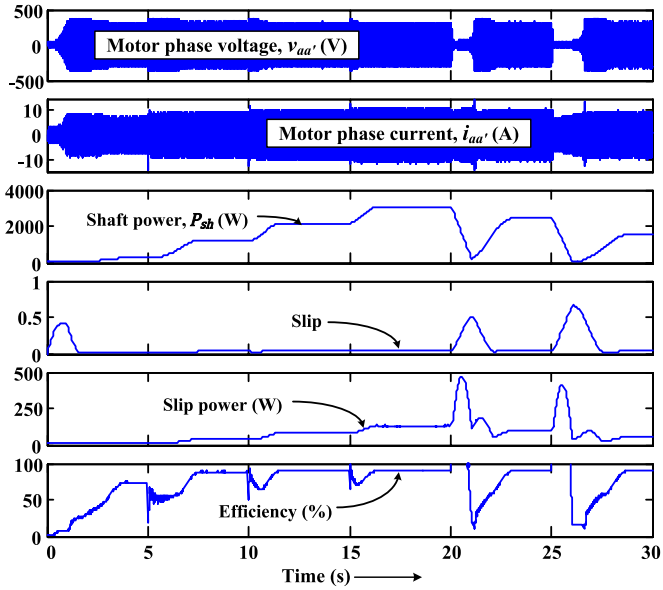

Fig. 9. OEWIM-side waveforms from simulation.

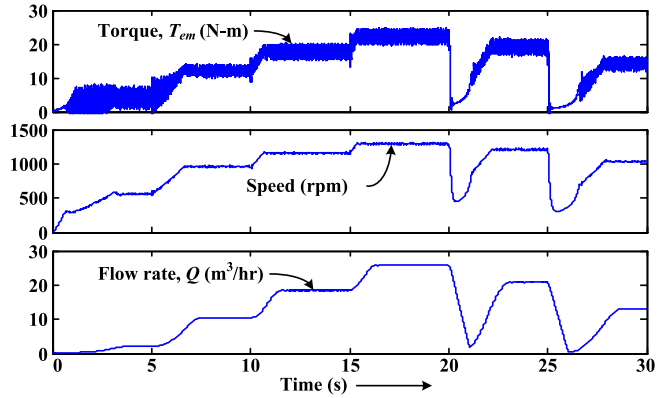

Fig. 10. Centrifugal-pump-side waveforms from simulation.

power subplot. Furthermore, it can be observed that PV voltage waveform shows a sudden rise and then fall in the value with the step increase and decrease in insolation and temperature. This can be attributed to the charging and the discharging of the PV capacitor with excess or deficit PV power, respectively, during transient condition.

The magnitude of the motor phase voltage shown in Fig. 9 follows the changes in the PV array voltage for various environmental conditions. In addition, the motor shaft power follows the extracted PV power (see Fig. 8). Furthermore, the motor slip power and the efficiency (calculated as the ratio of motor output power to the input power) increase with the increase in insolation. In addition, during sudden decrease in the insolation and temperature, the motor slip reaches a large value, which reduces the motor shaft power. This is because the PV power reduces significantly during this condition as the PV source operates in the current source region. It may be noted that the integrated algorithm could still handle these worst case environmental and operating conditions competently, and within few second(s), the system shows the tendency to settle and maintains the stability of the system. The stability of the

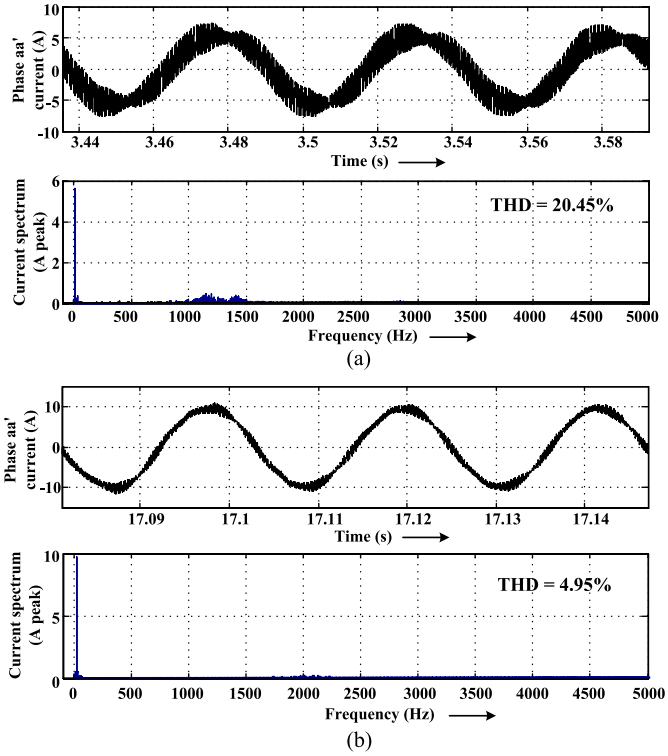

Fig. 11. Harmonic spectrum of motor phase current ($i_{aa'}$) at steady state obtained from simulation at different environmental conditions. (a) At 0.1 Suns and 25 °C. (b) At 1.0 Suns and 55 °C.

system can be ensured with the settled (constant) values of the PV parameters and the motor parameters for various insolation and temperature conditions. In the presented simulation studies, the environmental conditions are changed in steps, which may not be encountered in reality. This is to demonstrate the capacity of the proposed integrated control strategy.

The motor generated torque and speed and the water flow rate from the centrifugal pump are shown in Fig. 10. All these plots follow the same environmental conditions as aforementioned. The water flow rate is calculated by considering a constant head of 30 m. The last subplot in Fig. 10 shows a positive discharge even under the worst situations considered earlier. This proves that the proposed system could be a viable proposition even under worst environmental conditions for the applications where water can be stored and used later.

As the proposed system uses the SAZE PWM algorithm, the effect of zero-sequence current could be nullified, which can be proved by the sinusoidal nature of the motor phase current, as shown in Fig. 11. In addition, it can be observed that the ripple content in the current is more during lower insolation and the total harmonic distortion (THD) reduces as the insolation increases. Thus, in short, the system performance improves with increase in PV power. This can be observed in Table III, where the simulation results are summarized.

IV. Experimental Results

A prototype of the proposed system is developed to validate the simulation results and shown in Fig. 12. The solar PV array

TABLE III
SUMMARY OF SIMULATION RESULTS FOR THE PROPOSED SYSTEM

G Suns	T (°C)	PV Power (W)	Shaft Power (W)	η (%)	Speed (rpm)	Torque (N-m)	Slip (%)	Flow rate (m^3/hr)	Current THD (%)
0.1	25	329	239	72.64	560	4.2	1.82	2.05	20.45
0.4	35	1384	1221	88.22	962	12.1	2.95	10.45	16.04
0.5	40	1717	1528	88.99	1036	14.1	3.22	13.08	15.31
0.7	45	2406	2157	89.65	1161	17.8	3.65	18.46	8.88
0.8	50	2713	2429	89.53	1209	19.2	3.91	20.8	7.39
1	55	3368	3012	89.42	1298	22.2	4.26	25.78	4.95

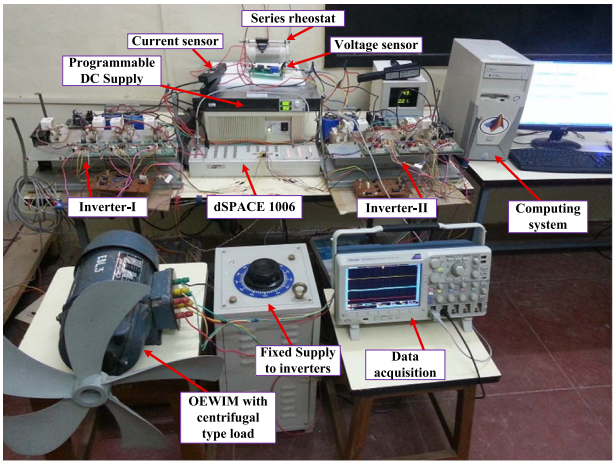

Fig. 12. Experimental prototype of the proposed system.

is emulated using a programmable dc power supply with a fixed series resistance. This arrangement could approximate the $P_{\rm pv}$ versus $V_{\rm pv}$ characteristics of the PV array. The programmable dc power supply is operated in constant voltage mode with a variable current limit. A 1-hp three-phase induction motor with stator windings open from both ends and with specifications of 440 V, 1.5 A, 1440 r/min is used in the experimental prototype. The shaft of the OEWIM is connected to a fan type of centrifugal load, which resembles the water pump. The motor is powered through the dual inverter, where the gate pulses required by the switches are generated from the signal controller dSPACE 1006. The controller includes the MPPT and SAZE PWM algorithms along with V/f control. The controller requires source voltage and current for implementing MPPT. To sense the source voltage and current, a Hall-effect voltage sensor (LV25-P) and a current sensor (Tektronix A622) are used, respectively. These voltage and current signals are given to the controller through the analog-to-digital converters (ADCs). Thus, two ADCs are sufficient to implement the proposed integrated algorithm. The waveforms captured from the experimental prototype are shown in Figs. 13 and 14.

Fig. 13 shows the source side and the controller parameters captured from the experimental setup. The modulation index m_a in the controller is set to a minimum value of 0.2, and a step change of 0.01 is considered to vary the value of m_a. The controller varies the value of m_a and aid the motor load to extract the maximum power possible from the source. The

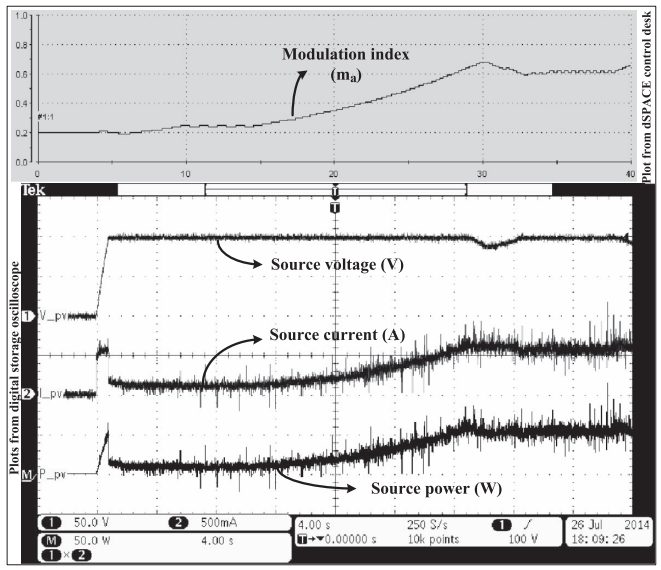

(a)

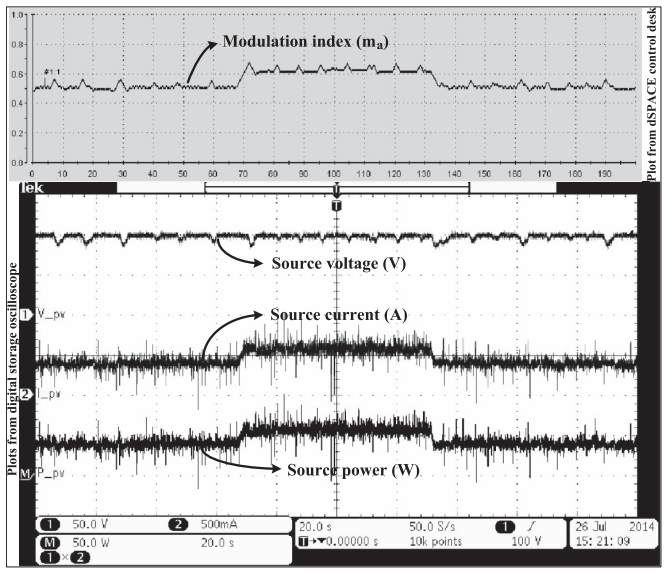

(b)

Fig. 13. Experimental results obtained from the developed prototype at dc source side, i.e., modulation index (0.2/div), source voltage (50 V/div), current (0.5 A/div), and power (50 W/div) (a) at starting condition (x-axis: 4 s/div) and (b) at running condition (x-axis: 20 s/div) with varying current limits (i.e., varying insolation values).

oscillatory nature of m_a, as shown in Fig. 13(a), demonstrates that the operating point is oscillating near MPP.

Fig. 13(b) shows the performance of the proposed integrated control strategy with a variable environmental condition. The variable environmental condition is emulated by varying the current limit of the programmable dc power supply from 0.4 to 0.6 A and then back to 0.4 A. The condition of lower insolation is emulated with lower current limit and vice versa. From Fig. 13(b), it is evident that the modulation index m_a and, hence, the source (PV) power adjust themselves as per the set current limit (insolation). It can be also observed that the value of m_a settles back to the previous value when the current limit is set back to 0.4 A. Thus, the system displays stability for both increasing and decreasing source (PV) power levels. The

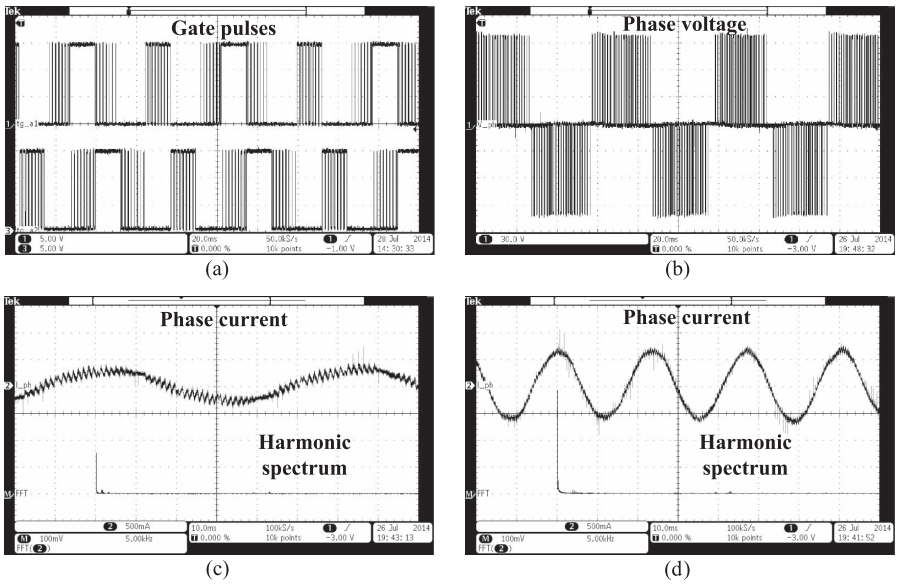

Fig. 14. Experimental results obtained from the developed prototype. (a) Gate pulses for poles a and a' of dual inverter (x-axis: 20 ms/div; y-axis: 5 V/div). (b) Motor aa'-phase voltage (x-axis: 20 ms/div; y-axis: 30 V/div); motor aa'-phase current (x-axis: 10 ms/div; y-axis: 0.5 A/div) and its harmonic spectrum (c) at starting condition and (d) at running condition.

experimental results shown in Fig. 13 are in good agreement with the simulation results shown in Fig. 8, validating the concept of the proposed integrated control strategy.

The working of the SAZE PWM technique and the V/f control can be observed from Fig. 14. The gate pulses shown in Fig. 14(a) are of poles a and a' (see Fig. 2) of inverter I and inverter II, respectively. The clamping and switching pattern verifies the implementation of the SAZE PWM technique, which could reduce the switching losses in the dual inverter. The nature of pole voltages is similar to the gate pulses, whereas the three-level phase voltage is shown in Fig. 14(b). The motor "aa'" phase current waveform and its harmonic spectrum at starting and running conditions are shown in Fig. 14(c) and (d), respectively. The harmonic spectrum at starting and running conditions is comparable with the harmonic spectrum of current at low and high insolation (see Fig. 11), respectively. It may be also noted that the pattern of ripple in the current waveform shown in Fig. 14(c) and (d) resembles the simulation results given in Fig. 11.

V. Conclusion

A single-stage system for PV power fed pump drive using an induction motor with open-end windings has been presented. The detailed design of the devices and components used in the proposed system is furnished. The proposed system is operated by an integrated control algorithm (MPPT + SAZE PWM with V/f control). This control algorithm has the capability of maintaining the system stability even under worst environmental situations, which is discussed and presented using the simulation studies. The simulation results are verified with the experimental results obtained from the developed low-scale prototype. In conclusion, a simple and effective PV pumping system has been presented in this paper, which is operated with an integrated control algorithm.

References

[1] A. Nabae, I. Takahashi, and H. Akagi, "A new neutralpoint-clamped PWM inverter," *IEEE Trans. Ind. Appl.*, vol. IA-17, no. 5, pp. 518–523, Sep./Oct. 1981.
[2] Y. Jiao, S. Lu, and F. C. Lee, "Switching performance optimization of a high power high frequency three-level active neutral point clamped phase leg," *IEEE Trans. Power Electron.*, vol. 29, no. 7, pp. 3255–3266, Jul. 2014.
[3] H. Stemmler and P. Guggenbach, "Configurations of high-power voltage source inverter drives," in *Proc. IEEE EPE*, 1993, pp. 7–12.
[4] K. Sivakumar, A. Das, R. Ramchand, C. Patel, and K. Gopakumar, "A hybrid multilevel inverter topology for an open-end winding induction-motor drive using two-level inverters in series with a capacitor-fed H-bridge cell," *IEEE Trans. Ind. Electron.*, vol. 57, no. 11, pp. 3707–3714, Nov. 2010.
[5] P. P. Rajeevan, K. Sivakumar, K. Gopakumar, C. Patel, and H. Abu-Rub, "A nine-level inverter topology for medium-voltage induction motor drive with open-end stator winding," *IEEE Trans. Ind. Electron.*, vol. 60, no. 9, pp. 3627–3636, Sep. 2013.
[6] V. T. Somasekhar, B. Venugopal Reddy, and K. Sivakumar, "A four-level inversion scheme for a six-n-pole open-end winding induction motor drive for an improved DC-link utilization," *IEEE Trans. Ind. Electron.*, vol. 61, no. 9, pp. 4565–4572, Sep. 2014.
[7] R. Sudharshan Kaarthik, K. Gopakumar, J. Mathew, and T. Undeland, "Medium-voltage drive for induction machine with multilevel dodecagonal voltage space vectors with symmetric triangles," *IEEE Trans. Ind. Electron.*, vol. 62, no. 1, pp. 79–87, Jan. 2015.
[8] B. Venugopal Reddy, V. T. Somasekhar, and Y. Kalyan, "Decoupled space-vector PWM strategies for a four-level asymmetrical open-end winding induction motor drive with waveform symmetries," *IEEE Trans. Ind. Electron.*, vol. 58, no. 11, pp. 5130–5141, Nov. 2011.
[9] B. Jacob and M. R. Baiju, "Vector-quantized space-vector-based spread spectrum modulation scheme for multilevel inverters using the principle of oversampling ADC," *IEEE Trans. Ind. Electron.*, vol. 60, no. 8, pp. 2969–2977, Aug. 2013.
[10] B. Jacob and M. R. Baiju, "A new space vector modulation scheme for multilevel inverters which directly vector quantize the reference space vector," *IEEE Trans. Ind. Electron.*, vol. 62, no. 1, pp. 88–95, Jan. 2015.
[11] A. Edpuganti and A. K. Rathore, "New optimal pulse width modulation for single dc-link dual inverter fed open-end stator winding induction motor drive," *IEEE Trans. Power Electron.*, vol. 30, no. 8, pp. 4386–4393, Aug. 2015.
[12] N. Bodo, E. Levi, and M. Jones, "Investigation of carrier-based PWM techniques for a five-phase open-end winding drive topology," *IEEE Trans. Ind. Electron.*, vol. 60, no. 5, pp. 2054–2065, May 2013.

[13] N. Bodo, M. Jones, and E. Levi, "A space vector PWM with common-mode voltage elimination for open-end winding five-phase drives with a single dc supply," *IEEE Trans. Ind. Electron.*, vol. 61, no. 5, pp. 2197–2207, May 2014.
[14] V. T. Somasekhar, S. Srinivas, B. Prakash Reddy, C. Nagarjuna Reddy, and K. Sivakumar, "Pulse width-modulated switching strategy for the dynamic balancing of zero-sequence current for a dual-inverter fed open-end winding induction motor drive," *IET Elect. Power Appl.*, vol. 1, no. 4, pp. 591–600, Jul. 2007.
[15] L. An and D. D.-C Lu, "Design of a single-switch dc/dc converter for a PV-battery-powered pump system with PFM+PWM control," *IEEE Trans. Ind. Electron.*, vol. 62, no. 2, pp. 910–921, Feb. 2015.
[16] M. A. Vitorino and M. B. Beltrão de Rossiter Corrêa, "An effective induction motor control for photovoltaic pumping," *IEEE Trans. Ind. Electron.*, vol. 58, no. 4, pp. 1162–1170, Apr. 2011.
[17] J. V. Mapurunga Caracas, G. de Carvalho Farias, L. F. Moreira Teixeira, and L. A. de Souza Ribeiro, "Implementation of a high-efficiency, high-lifetime and low-cost converter for an autonomous photovoltaic water pumping system," *IEEE Trans. Ind. Appl.*, vol. 50, no. 1, pp. 631–641, Jan./Feb. 2014.
[18] T. P. Corrêa, S. I. Seleme, Jr., and S. R. Silva, "Efficiency optimization in stand-alone photovoltaic pumping system," *J. Renew. Energy*, 41, pp. 220–226, May 2012.
[19] M. Taoufik, H. Karima, S. Lassaad, and G. Abdessattar, "Photovoltaic water pumping system with three-level NPC inverter," *Int. J. Eng. Sci.*, vol. 3, no. 10, pp. 99–108, Oct. 2014.
[20] S. Ozdemir, N. Altin, I. Sefa, and G. Bal, "PV supplied single stage MPPT inverter for induction motor actuated ventilation systems," *Elektronika ir Elektrotechnika*, vol. 20, no. 5, pp. 116–122, Jan. 2014.
[21] G. Walker, "Evaluating MPPT converter topologies using a MATLAB PV model," *J. Elect. Electron. Eng.*, vol. 21, no. 1, pp. 49–56, 2001.
[22] S. Jain and V. Agarwal, "Comparison of the performance of maximum power point tracking schemes applied to single-stage grid-connected photovoltaic systems," *IET Elect. Power Appl.*, vol. 1, no. 5, pp. 753–762, Sep. 2007.
[23] S. Jain and V. Agarwal, "A single-stage grid connected inverter topology for solar PV systems with maximum power point tracking," *IEEE Trans. Power Electron.*, vol. 22, no. 5, pp. 1928–1940, Sep. 2007.
[24] J.-S. Kim and S.-K. Sul, "A novel voltage modulation technique of the space vector PWM," in *Proc. IPEC*, 1995, pp. 742–747.
[25] D.-W. Chung, J.-S. Kim, and S.-K. Sul, "Unified voltage modulation technique for real-time three-phase power conversion," *IEEE Trans. Ind. Appl.*, vol. 34, no. 2, pp. 374–380, Mar./Apr. 1998.
[26] S. Srinivas and V. T. Somasekhar, "Space-vector-based PWM switching strategies for a three-level dual-inverter-fed open-end winding induction motor drive and their comparative evaluation," *IET Elect. Power Appl.*, vol. 2, no. 1, pp. 19–31, Jan. 2008.

Sachin Jain (M'15) received the B.E. degree from Bhilai Institute of Technology Durg, Pandit Ravishankar Shukla University, Durg, India, in 2000, the M.Tech. degree in integrated power systems from Visvesvaraya National Institute of Technology, Nagpur, India, in 2002, and the Ph.D. degree in electrical engineering from the Indian Institute of Technology Bombay, Mumbai, India, in 2008.

From 2007 to 2012, he was a Senior Design Engineer with the R&D Department, Solar Energy Business Group, Schneider Electric, Bangalore, India. He is currently an Assistant Professor with the National Institute of Technology Warangal, Warangal, India. His research interests include power electronic applications in nonconventional energy conditioning, power quality, and distributed generation.

Ramsha Karampuri received the B.Tech. degree from Srinivasa Ramanujan Institute of Technology, Jawaharlal Nehru Technological University, Hyderabad, India, and the M.Tech. degree from Visvesvaraya National Institute of Technology, Nagpur, India. He is currently working toward the Ph.D. degree in electrical engineering at the National Institute of Technology Warangal, Warangal, India.

His research interests include power electronics and drives, application of power electronics to nonconventional energy conditioning, and multiphase drives.

V. T. Somasekhar (M'11) received the Graduate degree from the Regional Engineering College Warangal (currently the National Institute of Technology Warangal), Warangal, India, in 1988, the Postgraduate degree from the Indian Institute of Technology Bombay, Mumbai, India, in 1990, and the Doctoral degree from the Indian Institute of Science, Bangalore, India, in 2003.

From 1990 to 1993, he was a Research and Development Engineer with Perpetual Power Technologies, Bangalore, and a Senior Engineer with Kirloskar Electric Company, Ltd., Mysore, India. Since 1993, he has been with the National Institute of Technology Warangal, where he is currently a Professor. His research interests include multilevel inversion with open-end winding induction motors, ac drives, and pulsewidth-modulation strategies.